Fiber Bragg grating sensor for simultaneous measurement of flow rate and direction

Ping Lu and Qiying Chen

Department of Physics and Physical Oceanography, Memorial University of Newfoundland, St John's,
NL A1B 3X7, Canada

E-mail: pinglu@mun.ca and qiyingc@mun.ca

Abstract

A new fiber-optic sensor system consisting of a fiber Bragg grating cantilever as a transducer is proposed and demonstrated to realize simultaneous measurement of fluid flow rate and direction. For the fiber Bragg grating mounted on either a stainless steel or a spring steel substrate, a change in the water flow rate gives rise to a monotonic shift in the Bragg resonance wavelength of the grating while the flow direction results in either a redshift or a blueshift in the Bragg wavelength due to a stretched or shrunk state of the grating. Shifts in the Bragg resonance wavelength of 0.077 and 0.826 nm at a water flow rate of 90 cm^3 s^{-1} were achieved with the fiber Bragg grating stainless steel and spring steel cantilever sensors, respectively. The experimental results are in good agreement with the theoretical analysis.

Keywords: optical fibers, fiber Bragg grating, sensor

(Some figures in this article are in colour only in the electronic version)

1. Introduction

Monitoring environmental parameters is crucial in manufacturing industries, environment and daily life. In many applications such as down-hole oil and ground piping systems in gas and oil industry, ocean tides in oceanography and water supply and sewage systems in urban infrastructure systems, *in situ* monitoring of fluid flow rate with innovative technologies of high accuracy, good reliability, cost effectiveness and ease of installation and operation is highly demanded [1]. However, in many harsh environments of high electromagnetic interference, high temperature, high pressure and high vibration, or the existence of toxic or corrosive agents, the traditional electrical flowmeters are not suitable. The fiber-optic sensor systems have exceeded these conventional counterparts with many unique advantages such as immunity to electromagnetic interference, compact sizes, potential low costs and the possibility of distributed measurement over a long distance [2]. Fiber-optic sensors have been reported as powerful sensors for many measurands including temperature, pressure, strain, salinity, mass flow rate and

rotation position [2–7]. Peng *et al* recently reviewed various fiber-optic flow sensors reported so far [8], which can be classified into three categories, i.e., vortex-shedding-based fiber-optic flow sensors, laser Doppler velocimeters and the interferometrically based fiber flow sensor with the modulation of low-coherence or speckle spectrum for flow detection. In addition, flow measurement based on fiber bending has also been reported [9, 10].

With the increasing interest in all-fiber systems, fiber-optic sensors utilizing fiber Bragg gratings (FBGs) have received considerable attention recently. The FBG sensors possess advantages such as wavelength encoded response, transmissive and/or reflective filtration, linear output, high sensitivity, large dynamic range and resolution, self-referencing, in-line optical connectivity, compatibility with fiber optical networks, wavelength division multiplexing (WDM) and time division multiplexing (TDM) capability. Lim *et al* developed an optical-based differential pressure flow sensor for an optically powered hydraulic valve monitoring and feedback control system [11]. Chen *et al* reported FBG gas flow sensors self-powered by in-fiber light [12, 13], in which the gas flow based on convective heat transfer principles

was measured by a thermal X-probe sensor consisting of two cross-mounted FBGs or by the self-heated optical hot wire anemometry of the FBGs.

In this paper, we present the first report on the simultaneous measurement of clean fluid flow rate and direction with a FBG sensor system while achieving temperature compensation. Determination of the direction of a flowing fluid is critical in many applications when the flow direction is not predictable such as ocean currents in oceanography or turbid fluids in many piping systems. However, the fiber-optic FBG fluid flow sensors reported so far have not achieved simultaneous measurement of the flow rate and direction yet. The key component of our sensor system is a FBG cantilever, which acts as the transducer. The sensing signal is the light coupled into the fiber from an external light source, which changes its optical properties when passing through the transducer. The set point, i.e., Bragg resonance wavelength, triggering time, responsivity and dynamic range of the sensor system, can be adjusted in order to satisfy the requirements of specific applications. The possibility of selecting a substrate material of different mechanical properties provides an additional capability to change the set point of the sensor on purpose. In the following sections, we will discuss the design and performance of our sensor system together with theoretical analysis and comparison with different flow sensors reported so far.

2. Theory

The Bragg resonance wavelength of a FBG, λ_B, can be expressed as

$$\lambda_B = 2n_{\text{eff}}\Lambda \tag{1}$$

where n_{eff} is the effective refractive index of the fiber core and Λ is the Bragg grating pitch.

The fractional wavelength shift, $\Delta\lambda_B$, corresponding to a temperature change ΔT can be written as [14]

$$\Delta\lambda_B = \lambda_B(\alpha + \zeta)\Delta T \tag{2}$$

where α is the thermal expansion coefficient of the fiber and ζ represents the thermo-optic coefficient.

The refractive index and thus the Bragg resonance wavelength are dependent on stress via the photo-elastic constants and the mechanically induced elongation. The term related to the strain effect may be expressed as [14]

$$\Delta\lambda_B = \lambda_B(1 - \hat{P}_e)\Delta\varepsilon \tag{3}$$

where $\Delta\varepsilon$ is the strain and $\Delta\lambda_B$ is the shift of the Bragg resonance wavelength. $\hat{P}_e$ is an effective strain optic constant with P_{11} and P_{12} as the strain tensor components related to axial loading, which is defined as

$$\hat{P}_e = \frac{n_{\text{eff}}^2}{2}[P_{12} - \upsilon(P_{11} + P_{12})] \tag{4}$$

where υ is the Poisson ratio.

If a FBG embedded fiber is mounted onto a steel plate cantilever to form a cantilever, the Bragg resonance wavelength of the FBG will redshift or blueshift when the cantilever experiences a convex or concave bending. For an

initial segment of the cantilever with an initial effective length of L, it becomes an arc with a corresponding angle θ and a final effective length of L' after convex bending. The fiber length changes from its initial value of l to l' after the convex bending of the fiber with a deflection value of D. The elongation length Δl of the fiber can be calculated using the geometric relations

$$\tan\left(\frac{\pi}{2} - \frac{\pi - \theta}{2}\right) = \frac{D}{L} \tag{5}$$

and

$$[2\pi(R + d) - 2\pi R] \cdot \frac{\theta}{2\pi} \cdot \frac{l}{L} = \Delta l \tag{6}$$

where d is the neutral axis distance between the optical fiber and cantilever.

After substituting (6) into (5), the relationship between Δl and D becomes

$$\Delta l = \frac{2dl}{L}\arctan\left(\frac{D}{L}\right). \tag{7}$$

Following (3), the redshift of the Bragg resonance wavelength induced by a convex bending is

$$\Delta\lambda_B = \frac{2d\lambda_B(1 - \hat{P}_e)}{L}\arctan\left(\frac{D}{L}\right). \tag{8}$$

On the other hand, the fiber will shrink when the cantilever experiences a concave bending, where the change in the fiber length and the position induced by the concave bending are symmetrical to the geometric relation with those induced by the convex bending as discussed above. Therefore, the shift in the Bragg resonance wavelength of the FBG induced by the concave bending has the same magnitude as that corresponding to the convex bending but with a different direction.

3. Experimental details

A standard telecommunication single-mode optical fiber (SMF-28, Corning Inc.) was soaked in high-pressure hydrogen atmosphere (1900 psi) at room temperature for 2 weeks and then stored in a freezer at $-70\,^\circ$C before use. Two FBGs with a grating length of 1 cm each were inscribed on the hydrogen-loaded fiber using an ArF excimer laser and phase masks. The experimental setup for inscribing the grating is shown in figure 1. After the grating fabrication, the FBG sample was baked at $150\,^\circ$C overnight to eliminate the residual hydrogen and the unstable UV-induced index changes. The grating areas were then recoated with acrylate polymer to protect the fiber. The transmission spectrum of the fiber inscribed with the two FBGs was measured by an optical spectrum analyzer (OSA, Ando 6315E) with a resolution of 0.05 nm, which shows Bragg resonance wavelengths at 1549.020 and 1550.268 nm with reflection signals of 9.24 and 8.90 dB, respectively (figure 2).

The schematic diagram of the water flow measurement with the FBG sensor system is shown in figure 3. Light emitted from an erbium broadband light source (EBS-7210, MPB Communications, Inc.) was received by the optical spectrum analyzer after passing through the FBGs. Two ends of the fiber for the grating at 1549.020 nm with the grating section at the center were attached to the two sides of a
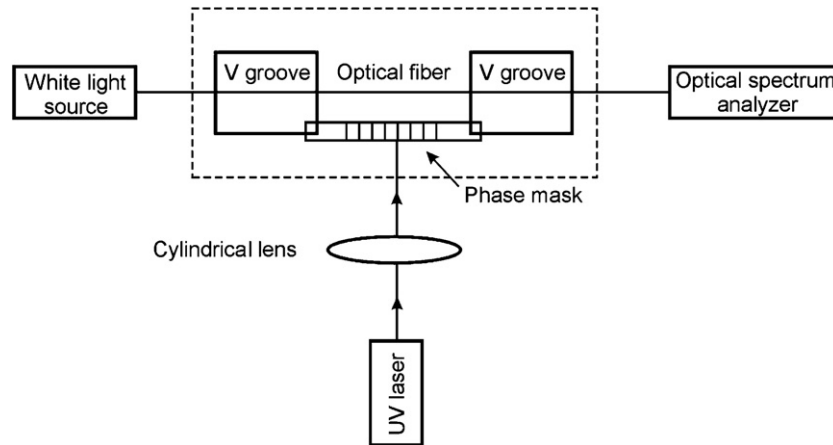
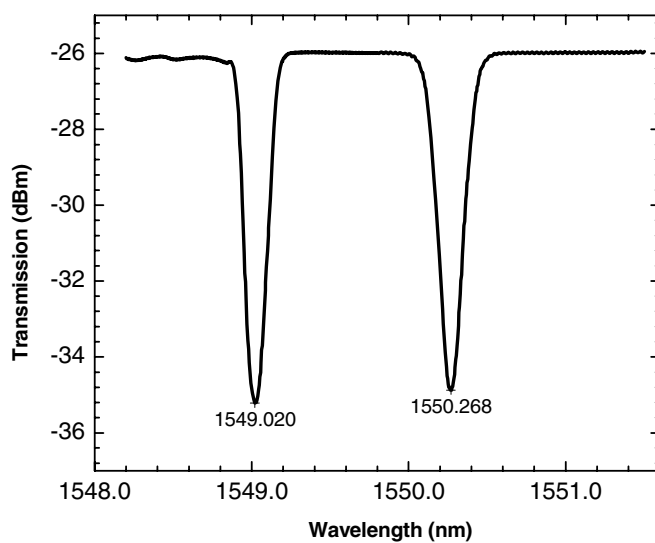**Figure 1.** Schematic diagram of a FBG fabrication setup.

Figure 2. Transmission spectrum of the free-standing fiber inscribed with two acrylate-coated FBGs at room temperature.

stainless steel or a spring steel plate cantilever using epoxy glue. During the process of mounting the fiber on the steel cantilever, the fiber was stretched in order to produce a pre-strained state. The set points of the pre-strained values for the FBG stainless steel and spring steel cantilever used in this study were both 50 $\mu\varepsilon$, which were carefully selected to ensure that no break and relative movement between the fiber cladding and its polymeric coating take place in the measurement. The top end of the cantilever was anchored onto a vertical frame with the bottom submerged in a water tank of 0.2 m in width and 1.4 m in length. The other FBG with the Bragg resonance wavelength at 1550.268 nm was fixed along the sidewall of the water tank to realize temperature compensation. Water emitted from an underwater nozzle of diameter 9.0 mm generated a flow flux up to 100 cm^3 s^{-1}, which induced bending of the FBG cantilever by the impact of the water flow. The experiments were performed in a wet bench (NU-WAVE 000218, Fineline Fabrications Inc., Ottawa, Canada) located in a temperature-controlled room with the temperature maintained at 20.0 $\pm$ 1.0 °C. A meterstick was attached on the side of the water tank

to measure the bending deflection of the cantilever. When a stream of water hits the cantilever toward the surface of the FBG, a convex bending of the cantilever is induced and the FBG stays in a stretched state. The FBG on the cantilever experiences a concave bending and stays in a shrunk state when a stream of water hits the opposite side of the cantilever.

4. Results and discussion

In our proposed scheme of FBG cantilever sensors, two types of steel cantilevers with different mechanical properties were used as the substrate for the FBG in separate water flow experiments: (1) a stainless steel (AISI 304) one, which undergoes a bending process when it is exposed to water impact, and (2) a spring steel (ASTM A228) one, which can return to its original shape despite significant bending due to its high yield strength.

4.1. Temperature compensation with a fiber Bragg grating

In order to solve the inherent cross-sensitivity effects of FBGs between temperature and strain, a temperature compensation technique using two different FBGs without hysteresis effects was adopted [4]. It is obvious that the FBG fixed on the water tank was only sensitive to temperature changes because it did not experience any bending effect. Figure 4 gives the Bragg wavelengths of the temperature monitoring FBG at different temperatures and flow rates. With its value of 1550.268 nm at the room temperature of 20 °C, the Bragg wavelength of the FBG showed a redshift with the increase in temperature indicating a temperature coefficient of 9.8 × 10^{-3} nm °C^{-1}. Details on the temperature measurement with a FBG can be found in our recent paper [5]. The temperature monitoring FBG shows a Bragg wavelength fluctuation of ±3 pm, corresponding to a temperature change of ±0.3 °C, with a variation in the fluid flow for a rate up to 90 cm^3 s^{-1}. In order to demonstrate the applicability of the FBG cantilever sensors proposed in this study and focus on the flow measurement, the environmental temperature is considered constant at 20 °C in the following investigation.
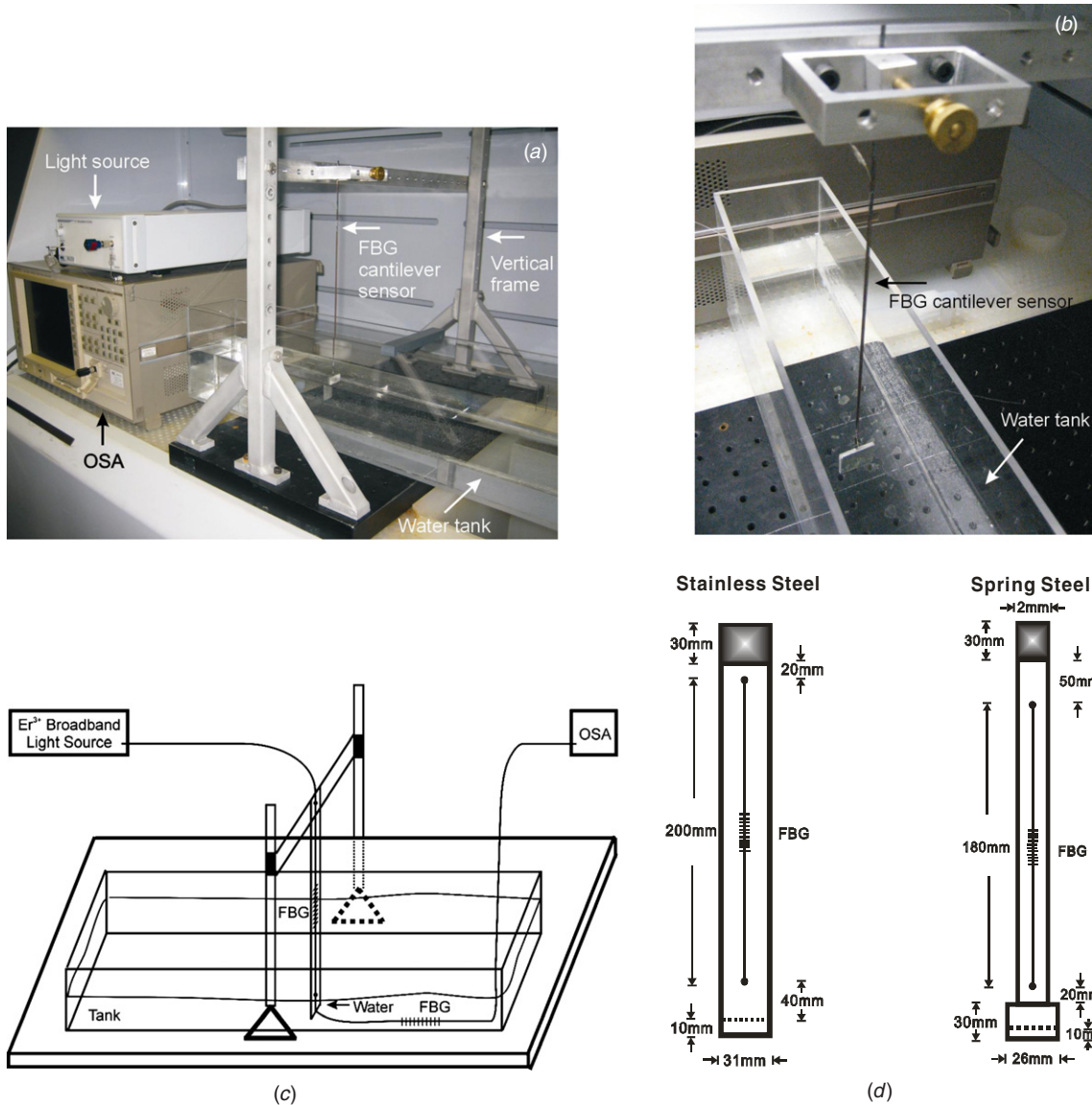
Figure 3. A FBG cantilever sensor system for fluid flow measurement with (*a*) a photo of the measurement system, (*b*) a photo of the FBG spring steel cantilever sensor, (*c*) schematic illustration of the measurement system and (*d*) schematic diagrams of the two FBG cantilever sensor systems with stainless steel and spring steel as the substrate, respectively.

4.2. Water flow measurement with a fiber Bragg grating stainless steel cantilever sensor

As illustrated in figure 3(*d*) for the FBG stainless steel cantilever, the top section (30 mm) of the cantilever was fixed and the bottom section (10 mm) was impacted by the water flow. The initial effective length of the cantilever was 260 mm with a fiber attaching length of 200 mm. First, the water flow hits the stainless steel cantilever on the side of the FBG (forward flowing case). During the process when the flow rate was increased from 0 to 90 cm³ s⁻¹, the corresponding transmission spectra of the FBG were recorded by the optical spectrum analyzer at different flow rates, as shown in figure 5(*a*). The process was repeated five times. Figure 5(*b*) gives the corresponding Bragg resonance wavelength of the FBG as a function of the flow rate. The change in the forward flow rate yielded an average wavelength shift of 0.077 nm with a standard deviation of 0.004 nm. When the flow rate was increased, the Bragg wavelength was found to shift toward a longer wavelength, which is consistent with the elongation of the FBG caused by the convex bending of the cantilever. When the water flow was changed to the opposite direction (backward flowing case) and the flow rate was increased from 0 to 90 cm³ s⁻¹, the Bragg wavelength of the FBG as a function of the water flow indicated an average wavelength shift of 0.027 nm with a standard deviation of 0.004 nm toward a shorter wavelength, which is consistent with the shrinkage of the FBG caused by the concave bending of the cantilever. Through linear regressions performed on experimental data in figure 5(*b*), the sensitivity of the forward flow 8.6 × 10⁻⁴ nm cm⁻³ s is found to be larger than that of the backward flow 3.0 × 10⁻⁴ nm cm⁻³ s. The difference in the sensitivity of the sensor for the two flow directions is mainly due to the pre-strained value adopted in the experiment. It is possible to obtain a symmetric wavelength shift as a function of the
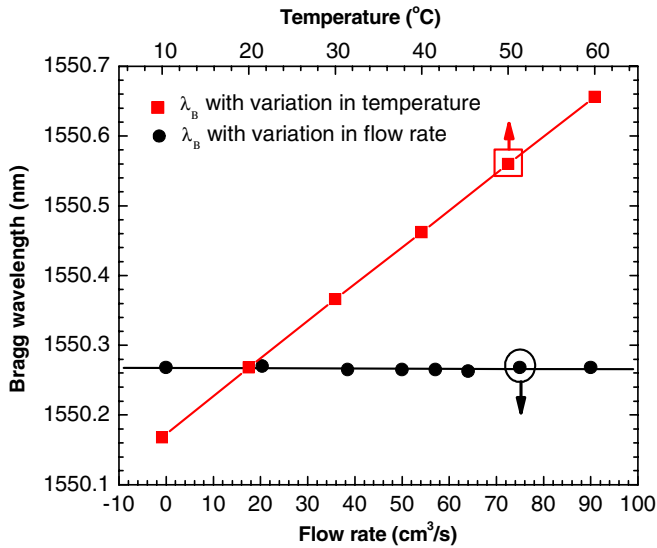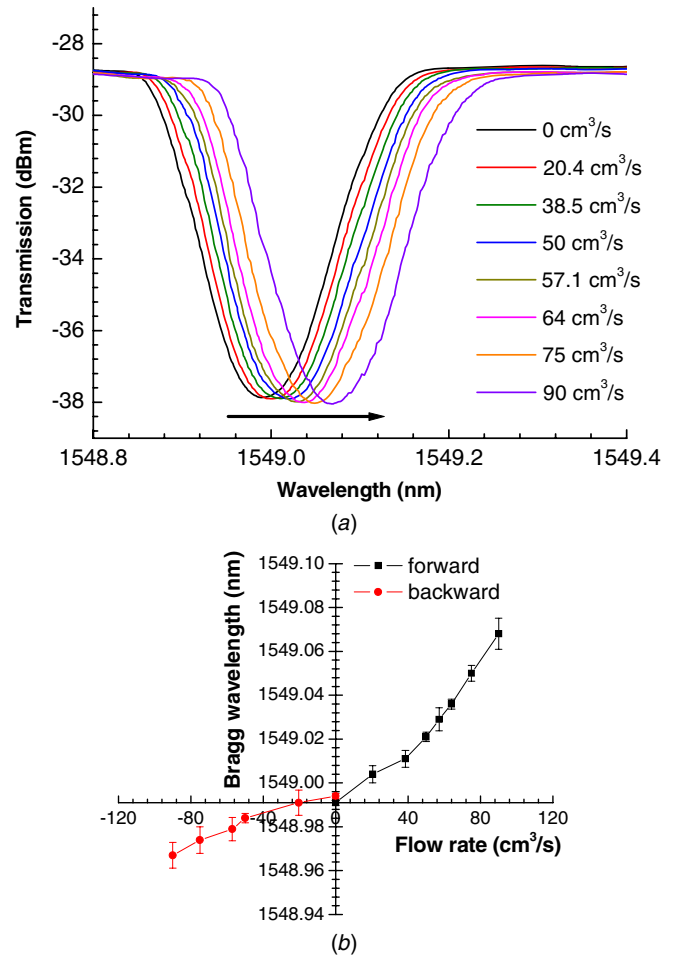
Figure 4. Bragg resonance wavelength of the FBG for temperature monitoring: ●, change in the Bragg wavelength with variation in flow rate at a constant temperature of $20.0 \pm 1.0\,^\circ\text{C}$; ■, change in the Bragg wavelength with variation in the environmental temperature.

water flow rate under forward and backward flows at some pre-strained values. However, it is quite difficult to tension the fiber sufficiently in this fiber cantilever configuration either for the stainless steel or for the spring steel. The asymmetric wavelength shift offers an indication that the direction of the fluid flow has changed. Repeated measurements on the cantilever sensors indicated that the sensing response was reproducible without the hysteresis effect. The resolutions for the forward and backward flow measurements in this FBG stainless steel cantilever are 58.1 and 166.7 $\text{cm}^3\,\text{s}^{-1}$, respectively. The monotonic dependence of the shift of the Bragg resonance wavelength on the flow rate as well as its redshift or blueshift corresponding to the forward or backward flowing cases as indicated in figure 5 clearly demonstrates that the FBG stainless steel cantilever is an effective transducer to realize simultaneous sensing of the water flow both for its rate and direction.

In order to analyze the experimentally observed increase in the Bragg wavelength induced by the forward water flow, a simulation was performed by using (8). For the FBG in the stainless steel cantilever sensor, the neutral axis distance d was measured to be 250 μm from optical microscopy. Both the experimental deflection of the cantilever induced by the forward water flow and the calculated Bragg wavelength corresponding to the fiber convex bending effect as functions of the flow rate are shown in figure 6. It was found that the observed deflection of the stainless steel cantilever was 9 mm at a water flow of 90 $\text{cm}^3\,\text{s}^{-1}$ and the calculated redshift of the FBG resonance peaks is 0.081 nm, which is in good agreement with the experimental result of 0.077 nm.

4.3. Water flow measurement with a fiber Bragg grating spring steel cantilever sensor

For a separate approach in which a spring steel cantilever was adopted, a schematic diagram of the sensor is illustrated in
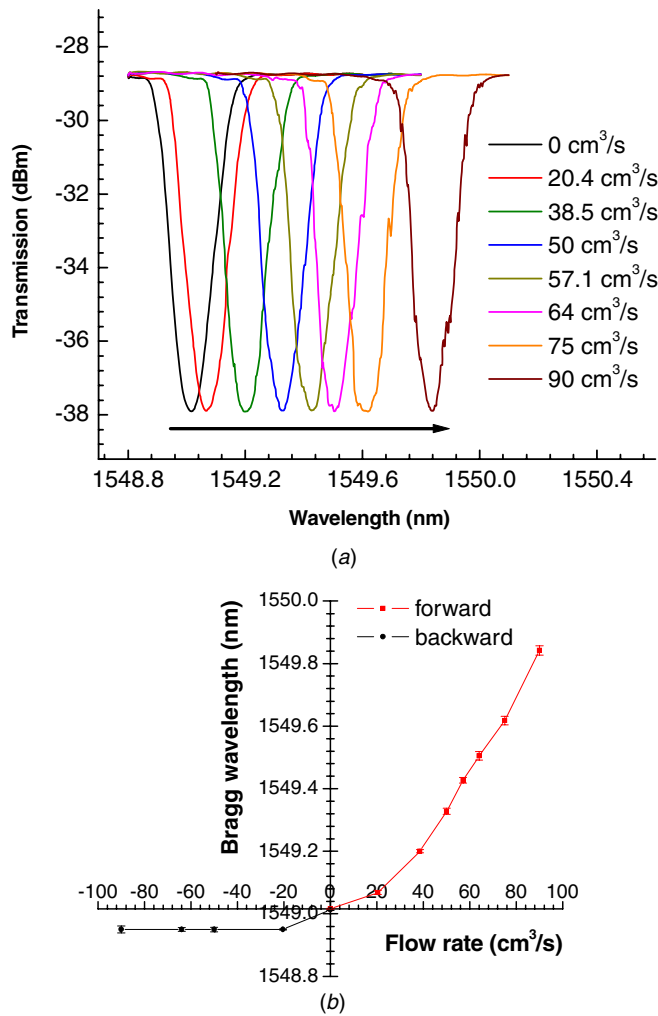

(a)

(b)

Figure 5. Bragg resonance wavelength of the FBG stainless steel cantilever sensor as a function of the water flow rate with (a) shift of the transmission spectrum under the forward flow and (b) shift of the Bragg wavelength in both the forward and the backward flows.
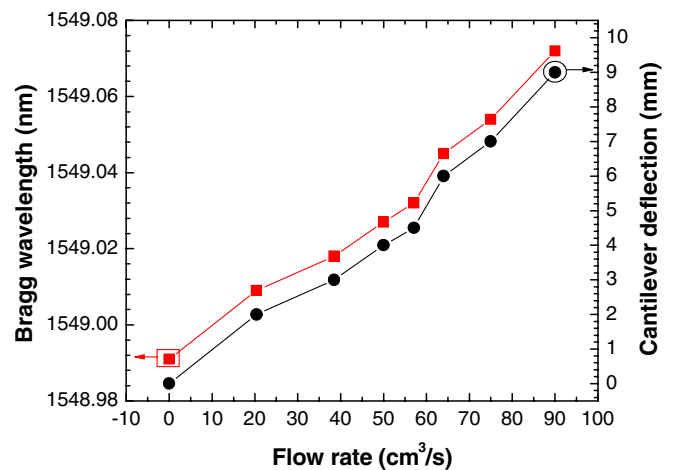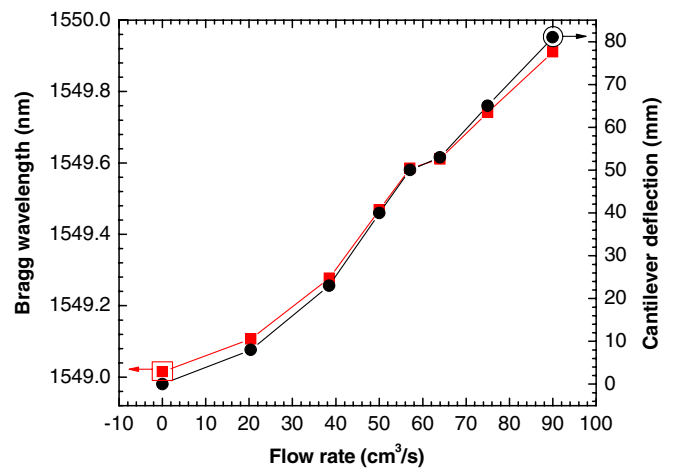

Figure 6. Experimentally measured bending deflections and the simulation of the corresponding Bragg resonance wavelengths of the FBG stainless steel cantilever at different flow rates: ●, experimental bending deflections; ■, simulation of the corresponding Bragg resonance wavelengths due to the convex bending.

figure 3(d). An aluminum plate of length 30 mm and width 26 mm was jointed on the base of the cantilever to increase the

(a)

(b)

Figure 7. Bragg resonance wavelength of the FBG spring steel
cantilever sensor as a function of the water flow rate with (a) shift of
the transmission spectrum under the forward flow and (b) shift of
the Bragg wavelength in both the forward and the backward
flows.

impact area and stabilize the slender cantilever. A section of
180 mm fiber was mounted on the cantilever. The top section
(30 mm) of the cantilever was fixed on the frame and the
bottom section of the aluminum board (10 mm) was pushed by
the flowing water. The initial effective length of the cantilever
was 270 mm. Figure 7(a) displays the transmission spectra
of the FBG when the forward water flow rate was increased
from 0 to 90 cm^3 s^{-1}. As the flow rate is increased, the
Bragg wavelength shifts toward longer wavelength, which is
consistent with the elongation of the FBG caused by the convex
bending of the spring steel cantilever. When the water flow was
changed to the opposite direction (backward flowing case) and
the flow rate was increased from 0 to 90 cm^3 s^{-1}, the average
FBG Bragg wavelength over five separate measurements
was adopted to remove random disturbance from the water
flow with its dependence on water flow rate, as shown in
figure 7(b), together with the standard deviation. When the
water flow rate reached about 20 cm^3 s^{-1}, no further shift
in the Bragg wavelength was observed due to the complete
relaxation of the fiber. The change in the forward water

Figure 8. Experimentally measured bending deflections and the
simulation of the corresponding Bragg resonance wavelengths of the
FBG spring steel cantilever at different flow rates: ●, experimental
bending deflections; ■, simulation of the corresponding Bragg
resonance wavelengths due to the convex bending.

flow rate yielded an average wavelength shift of 0.826 ±
0.009 nm. The sensitivity and resolution of the forward flow
are 9.2 × 10^{-3} nm cm^{-3} s and 5.4 cm^3 s^{-1}, respectively.
To compare the experimental results with the simulation, the
deflections of the cantilever induced by the increasing flow
rate were recorded in figure 8. The neutral axis distance d
was measured to be 340 μm and a cantilever deflection of
81 mm was observed at a forward water flow rate of 90 cm^3 s^{-1}.
Figure 8 indicates that the simulated redshift in the Bragg
wavelength from (8) is 0.896 nm. The difference in the
experimental result of 0.826 nm is believed to originate from
the vibration of the spring steel cantilever standing in the
changing water stream, which results in the unstable Bragg
resonance wavelength of the FBG.

*4.4. Comparison between the two fiber Bragg grating
cantilever sensors and other reported flow sensors*

The measured bending deflection ratio is 81:9 for the spring
steel and stainless steel cantilevers. In the forward flowing
case with a flow rate of 90 cm^3 s^{-1}, the Bragg wavelength
shifts of 0.826 and 0.077 nm were experimentally observed
for the FBG spring steel and stainless steel cantilever sensors,
respectively, which indicate a ratio of 11. From (8), the ratio
of the Bragg resonance wavelength shifts of the two FBGs
induced by the cantilever deflection is calculated to be 11.
Table 1 summarizes the measured results of the two FBG
cantilever sensors in comparison with the simulation results,
which indicates good agreement. The spring steel cantilever
with a small width brings more bending deflection under the
same water impact than the stainless steel one with a large
width. Thus, the spring steel cantilever sensor is more suitable
for slow water flow measurement for its higher sensitivity.
Furthermore, the sensitivity of the FBG water flow sensor
can be enhanced by an increase in the neutral axis distance
d and selection of the set point of the pre-strained value for
the FBG cantilever. Two major sources of uncertainty are the

Table 1. Experimental and simulation results of the FBG stainless steel and the spring steel cantilever flow sensors in this study.

Parameter	Stainless steel (AISI 304)	Spring steel (ASTM A228)	Ratio
Sensitivity ($nm\ cm^{-3}\ s$)	8.6×10^{-4} (forward flow) 3.0×10^{-4} (backward flow)	9.2×10^{-3} (forward flow)	–
Resolution ($cm^3\ s^{-1}$)	58.1 (forward flow) 166.7 (backward flow)	5.4 (forward flow)	–
Deflection (mm) (experimental)	9	81	9
Shift in Bragg wavelength (nm) (experimental)	0.077	0.826	11
Shift in Bragg wavelength (nm) (simulation)	0.081	0.896	11

Table 2. Comparison of the FBG cantilever flow sensors with other reported flow sensors.

Parameter	Electrical fluid flow-meter [15]	Vortex shedding fiber-optic flow sensor [16]	Fiber-optic interferometric flow sensor [8]	FBG differential pressure flow sensor [11]	FBG cantilever flow sensors (this study)
Measurement of flow rate	Yes	Yes	Yes	Yes	Yes
Sensitivity	–	–	–	$2.0 \times 10^{-4}\ nm\ cm^{-3}\ s$ (for flow rate $<200\ cm^3\ s^{-1}$)[a]; $6.3 \times 10^{-4}\ nm\ cm^{-3}\ s$ (for flow rate between 200 and $800\ cm^3\ s^{-1}$)[a]	For stainless steel cantilever, $8.6 \times 10^{-4}\ nm\ cm^{-3}\ s$ (forward flow); $3.0 \times 10^{-4}\ nm\ cm^{-3}\ s$ (backward flow). For spring steel cantilever, $9.2 \times 10^{-3}\ nm\ cm^{-3}\ s$ (forward flow)
Resolution	$2–550\ cm^3\ s^{-1}$	$0.2\ m\ s^{-1}$	$1.9\ cm^3\ s^{-1}$	$150\ cm^3\ s^{-1}$ (for flow rate $<200\ cm^3\ s^{-1}$)[a]; $47.6\ cm^3\ s^{-1}$ (for flow rate between 200 and $800\ cm^3\ s^{-1}$)[a]	For stainless steel cantilever, $58.1\ cm^3\ s^{-1}$ (forward flow); $166.7\ cm^3\ s^{-1}$ (backward flow). For spring steel cantilever, $5.4\ cm^3\ s^{-1}$ (forward flow)
Measurement of flow direction	No	No	No	No	Yes
Temperature compensation	No	No	Yes	Yes	Yes
Possibility of quasi-distributed measurement	No	No	No	Yes	Yes
Signal attenuation	Low	High	Low	Low	Low
Application in harsh environment	No	Yes	Yes	Yes	Yes

[a] Calculated from figure 8 of [11]; –, data not available.

negligible temperature fluctuation and Bragg wavelength shift measurement. If the sensor is placed in a full open channel flow, the large bulk of uniformly moving liquid may dampen some of the oscillations of the cantilever and decrease the uncertainty.

The novelty of this paper is that it is the first report on the simultaneous measurement of fluid flow rate and direction with a possible temperature compensation mechanism realized by a FBG sensor system. A comparison between the FBG cantilever sensors developed in this study and other reported

flow sensors is listed in table 2, which indicates larger sensitivity and better resolution of the FBG cantilever sensor discussed here with the advantages of direction measurement, temperature compensation, possibility of quasi-distributed measurement and applications in harsh environment.

5. Conclusion

In summary, a new scheme to realize simultaneous measurement of flow rate and direction with temperature compensation has been developed. The fiber-optic sensor system consists of two acrylate-coated FBGs with one for temperature monitoring and the other incorporated with a supporting substrate as a cantilever sensor for flow measurement. For the FBG stainless steel or spring steel cantilever sensors used in this study, shifts of 0.077 and 0.826 nm in the Bragg resonance wavelength of the FBG at a water flow rate of 90 cm^3 s^{-1} at room temperature were observed, respectively. The optical sensing was achieved by light propagation through the gratings with the advantages of adjustable set point, short triggering time, fast responsivity and large dynamic range. The adoption of a cantilever structure provides an additional capability to change the performance of the sensor system in addition to the obvious benefit of protection to the fiber. The experimental results are in good agreement with the theoretical analysis. This new sensing technique has the merits of simplicity in the sensing principle, ease of fabrication and low cost. It is also possible to apply this sensor as a shape sensor or a smart structure sensor.

Acknowledgments

References

[1] Baker R C 2005 *Flow Measurement Handbook: Industrial Designs, Operating Principles, Performance, and Applications* (Cambridge: Cambridge University Press)

[2] Kuzyk M G 2006 *Polymer Fiber Optics: Materials, Physics, and Applications* (Boca Raton, FL: CRC)

[3] Ho Y-T, Huang A-B and Lee J-T 2008 Development of a chirped/differential optical fiber Bragg grating pressure sensor *Meas. Sci. Technol.* **19** 045304

[4] Lu P, Men L and Chen Q 2008 Resolving cross sensitivity of fiber Bragg gratings with different polymeric coatings *Appl. Phys. Lett.* **92** 171112

[5] Men L, Lu P and Chen Q 2008 A multiplexed fiber Bragg grating sensor for simultaneous salinity and temperature measurement *J. Appl. Phys.* **103** 053107

[6] Rahim R A, Green R G, Horbury N, Dickin F J, Naylor B D and Pridmore T P 1996 Further development of a tomographic imaging system using optical fibres for pneumatic conveyors *Meas. Sci. Technol.* **7** 419–22

[7] Montanini R and Pirrotta S 2006 A temperature-compensated opto-mechanical rotational position sensor based on fibre Bragg gratings *Sensors Actuators* A **132** 533–40

[8] Peng W, Pickrell G R, Xu J, Huang Z, Kim D W, Qi B and Wang A 2004 Self-compensating fiber optic flow sensor system and its field application *Appl. Opt.* **43** 1752–60

[9] Nemoto T, Hashimato Y, Sato S and Iitaka H 1998 An optical fiber flow speed sensor of increased sensitivity *Electr. Eng. Japan* **125** 1–8

[10] Fang J X, Taylor H F and Choi H S 1998 Fiber-optic Fabry–Perot flow sensor *Microw. Opt. Technol. Lett.* **18** 209–11

[11] Lim J, Yang Q P, Jones B E and Jackson P R 2001 DP flow sensor using optical fiber grating *Sensors Actuators* A **92** 102–8

[12] Jewart C, McMillen B, Cho S K and Chen K P 2006 X-probe flow sensor implemented through the use of active fiber-Bragg gratings *Sensors Actuators* A **127** 63–8

[13] Cashdollar L and Chen K P 2005 Active fiber optical flow sensor *IEEE Sensors J.* **5** 1327–31

[14] Meltz G and Morey W W 1991 Bragg grating formation and germanosilicate fiber photosensitivity *Proc. SPIE* **1516** 185–99

[15] Sanderson M L 1994 Domestic water metering technology *Flow Meas. Instrum.* **5** 107–13

[16] Webster S, McBride R, Barton J S and Jones J D C 1992 Air flow measurement by vortex shedding from multimode and monomode optical fibres *Meas. Sci. Technol.* **3** 210–6